

Evaluating Cell Type Inference in Vision Language Models Under Varying Visual Context

Samarth Singhal
University of North Dakota
samarth.singhal@und.edu

Sandeep Singhal
University of North Dakota
sandeep.singhal@und.edu

Abstract

Vision-Language Models (VLMs) have rapidly advanced alongside Large Language Models (LLMs). This study evaluates the capabilities of prominent generative VLMs, such as GPT-4.1 and Gemini 2.5 Pro, accessed via APIs, for histopathology image classification tasks, including cell typing. Using diverse datasets from public and private sources, we apply zero-shot and one-shot prompting methods to assess VLM performance, comparing them against custom-trained Convolutional Neural Networks (CNNs). Our findings demonstrate that while one-shot prompting significantly improves VLM performance over zero-shot ($p \approx 1.005 \times 10^{-5}$ based on Kappa scores), these general-purpose VLMs currently underperform supervised CNNs on most tasks. This work underscores both the promise and limitations of applying current VLMs to specialized domains like pathology via *in-context learning*. All code and instructions for reproducing the study can be accessed from the repository [GitHub](#).

1. Introduction

Recent advancements in Vision-Language Models (VLMs) [1, 21], which process both visual and textual information, have spurred significant progress. Early foundational VLMs like CLIP [21] focused primarily on learning powerful joint image-text representations. More recently, a new generation of sophisticated VLMs, including models like GPT-4V [18], Gemini [6], and InternVL [5], have demonstrated remarkable capabilities in understanding and generating content based on complex multimodal inputs. Crucially, these advanced VLMs can follow intricate instructions interleaved with images and text, enabling direct application to tasks like visual question answering and prompted classification.

Deep learning has revolutionized computational pathology, yet state-of-the-art classifiers require thousands of labeled examples and costly re-training for each new

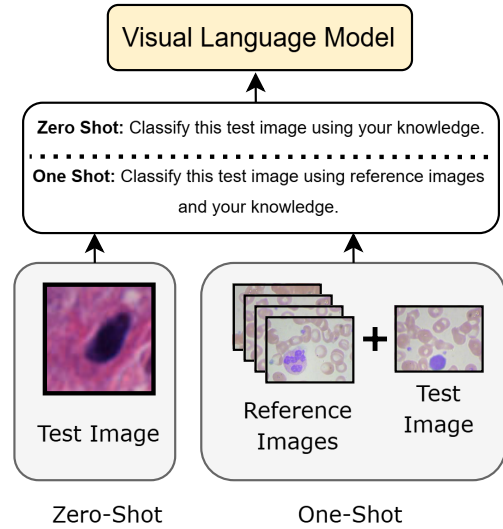


Figure 1. Evaluation Pipeline for Generative VLMs

biomarker, stain, or organ [12]. Despite these gains, three persistent bottlenecks hamper widespread adoption.

Data scarcity: Every new diagnostic question demands a fresh cohort of meticulously annotated images [10], an onerous burden for already over-extended pathology services.

Compute barriers: Fine-tuning large vision backbones for each task is compute-intensive and often beyond the reach of smaller research groups or hospitals [3, 16].

Limited knowledge integration: Classical CNNs operate solely on pixels, failing to exploit the rich textual and clinical context [22] that accompanies histology slides.

Recent work in *in-context learning* (ICL) [8] shows that large language models can generalize from only a handful of examples provided at inference time [4, 17]. Building on these advances, we adapt the ICL paradigm to pathology images, specifically for cell and tissue classification. We test two prompt regimes—**zero-shot** and **one-shot**—using state-of-the-art **Vision-Language Models (VLMs)** such as

GPT-4.1, Gemini 2.5 Pro, InternVL 3, and GPT-4.1 Mini, selected for their ability to process interleaved image-text prompts and follow instructions. We also evaluate the medical domain-specific VLM, *LLaVA-Med* [11] in our study. Our experiments extend ICL to vision–language pathology tasks and provide the first head-to-head comparison of these current general-purpose VLMs under both settings. Crucially, we treat these models as *unmodified* foundations—*not* clinical tools—to (i) quantify their “as is” performance via prompting, and (ii) identify gaps that a dedicated medical VLM and/or Agent [20] might need to address.

2. Methods

2.1. Evaluation Pipeline

Fig. 1 schematically illustrates the ordering of images and text inside every inference prompt. Approximately 200 images were used per class for testing across all datasets. Each call embeds both modalities in a single message constructed in one of two regimes:

Zero-shot: The prompt contains only the query image followed by

```
``Classify this test image based on your
knowledge alone. Choices: <c1>, ..., <cK>.
Reply with the class name in one or two
words maximum.``
```

This measures the innate pathology knowledge of an unmodified VLM.

One-shot: For every class c_k we first insert exactly one reference image and its caption

```
``This image is class: c_k``.
```

After the K exemplars we append the query image and instruct

```
``Now classify this test image using
reference images and your knowledge.
Choices: <c1>, ..., <cK>. Reply with the class
name in one or two words maximum.``
```

The explicit enumeration of class names enforces a closed-set decision while enabling the model to combine visual cues from the exemplars with its pretrained medical priors.

2.2. Datasets

Our benchmarks draw on a diverse collection of histopathology image sets that vary in tissue origin, staining protocol, and annotation granularity. Table 1 summarizes dataset specifics, including class counts and average image dimensions (in pixels).

We utilized several existing datasets, all used *as published* without requiring additional preprocessing. These include: **Blood Cell Count and Detection (BCCD)** [15]—providing 12,500 augmented peripheral blood

smear images with four leukocyte class labels; **Matek *et al.*** [13]—containing bone-marrow cytology images (May-Grünwald-Giemsa/Pappenheim stain) with ten bone-marrow cell class labels; and the **Meng *et al.*** tissue dataset [14] (time-stretch microscopy), which ships pre-segmented images and three phenotype labels.

The **Private Bladder** dataset (collected under IRB approval) includes 3 Hematoxylin and Eosin (H&E) whole-slide images (WSIs) at 40x magnification from 3 deidentified patients with urothelial carcinoma. Each WSI represents a unique patient and was assigned a distinct tumor aggressiveness grade (1, 2, or 3) by a certified pathologist, who delineated broad tumor and non-tumor regions. This dataset supports two derived tasks: (1) **Tumor Grading Classification:** using patches sampled from regions corresponding to the pathologist-assigned grade for each WSI. (2) **Cell-Type Classification:** distinguishing tumor vs. non-tumor nuclei. For this, nuclei within the pathologist-delineated regions were first segmented using QuPath [2] (hematoxylin channel analysis), and then 10,000, 250x250 pixel patches centered on these nuclei were extracted *per class* (i.e., 10k tumor nuclei patches, 10k non-tumor nuclei patches).

PanNuke [9] contains H&E patches spanning 19 tissue types. We leveraged its nucleus segmentation masks to isolate individual cells: bounding boxes were placed around each mask and cropped to fixed-size patches, yielding balanced sets of neoplastic, inflammatory, connective, dead, and epithelial nuclei.

Together these collections cover cytology, surgical pathology, and nuclear phenotyping under multiple class cardinalities, providing a rigorous test bed for zero-shot and one-shot vision–language inference.

Dataset	Classes	Tissue	Avg. Pixel Size
Bladder Tumor	2	Bladder	64x64
Meng <i>et al.</i> [14]	3	Blood and Breast	128x128
Bladder Grade	3	Bladder	280x280
BCCD [15]	4	Blood	320x240
PanNuke [9]	5	Various Tissues	46x46
Matek <i>et al.</i> [13]	10	Bone Marrow	250x250

Table 1. Dataset Overview

2.3. Models

We evaluated a spectrum of models ranging from a traditional Convolutional Neural Network (CNN) [19] baseline to several state-of-the-art Vision-Language Models (VLMs), applying the zero-shot and one-shot prompting strategies described in Tab. 2 without any model fine-tuning for the VLMs.

Custom CNN: As a baseline, we trained a standard CNN with three sequential Conv3x3-ReLU-MaxPool blocks fol-

lowed by a dense classifier head. This model was trained conventionally on the respective dataset tasks, using training sets containing, on average, at least 6000 images per class where applicable.

Vision-Language Models (VLMs): We assessed the following large pre-trained models accessed via their APIs or standard implementations:

- **Gemini 2.5 Pro [6]:** A leading closed-source multimodal model from Google, recognized for its number one spot on huggingface VLM leaderboard [7] benchmarks at the time of evaluation.
- **GPT-4.1 [18]:** The latest flagship large multimodal model release from OpenAI.
- **GPT-4.1 Mini:** A smaller, potentially more efficient variant of OpenAI’s GPT-4.1 model.
- **InternVL [5]:** A prominent open-source VLM known for strong performance across various vision-language tasks.
- **LLaVA-Med [11]:** A VLM specifically adapted for the general medical domain, evaluated to assess potential benefits of domain-specific pre-training.

These VLMs were used directly as foundation models to evaluate their inherent capabilities for pathology image understanding through in-context learning prompts.

2.4. Evaluation Metrics

We quantified model performance using three established classification metrics: Accuracy, Macro-averaged F1-score, and Cohen’s Kappa coefficient.

Accuracy measures the overall proportion of correctly classified instances:

$$\text{Accuracy} = \frac{\text{Number of Correct Predictions}}{\text{Total Number of Predictions}} \quad (1)$$

Macro-averaged F1-score computes the harmonic mean of precision and recall independently per class, then averages these scores uniformly across all classes. This approach gives equal importance to each class irrespective of class distribution:

$$\text{F1}_{macro} = \frac{1}{N} \sum_{i=1}^N 2 \cdot \frac{\text{Precision}_i \cdot \text{Recall}_i}{\text{Precision}_i + \text{Recall}_i} \quad (2)$$

where N represents the total number of classes.

Cohen’s Kappa evaluates the classification agreement adjusted for chance:

$$\kappa = \frac{p_o - p_e}{1 - p_e} \quad (3)$$

where p_o is the observed accuracy and p_e is the expected accuracy due purely to chance agreement.

Together, these metrics provide a comprehensive quantitative assessment of each model’s predictive reliability, class-balanced accuracy, and consistency beyond random chance, ensuring rigorous comparative analysis.

3. Results

We evaluated the performance of a baseline CNN and several state-of-the-art VLMs under zero-shot and one-shot prompting regimes across six distinct histopathology classification tasks. The detailed performance metrics (Accuracy, Macro F1-score, Cohen’s Kappa) are presented in Table 2.

Overall, the supervised CNN model consistently achieved the highest performance across most datasets, establishing a strong benchmark, particularly on Bladder Grade ($\kappa=0.985$), Bladder Tumor ($\kappa=0.920$), Matek *et al.* ($\kappa=0.748$), Meng *et al.* ($\kappa=0.830$), and PanNuke ($\kappa=0.440$). VLMs in the zero-shot setting generally struggled, often performing near or below chance levels, indicated by Kappa values close to or below zero (e.g., GPT 4.1 on Bladder Tumor: $\kappa=0.005$; Gemini 2.5 Pro on Bladder Grade: $\kappa=-0.004$).

One-shot prompting significantly boosts VLM performance. Comparing the zero-shot and one-shot results for the four VLMs across all six datasets reveals a substantial improvement when a single example per class is provided, particularly evident in the Cohen’s Kappa scores. For instance, GPT 4.1’s Kappa on Bladder Grade improves from 0.040 (zero-shot) to 0.393 (one-shot), and InternVL3’s Kappa on Bladder Tumor increases from 0.235 to 0.315. To statistically validate this observation, we performed a *one-sided paired Wilcoxon signed-rank test* comparing the zero-shot and one-shot Kappa scores across all VLM-dataset pairs ($N=24$). The results confirm a highly significant improvement with one-shot prompting ($p \approx 1.005 \times 10^{-5}$), demonstrating the effectiveness of minimal in-context learning for enhancing VLM performance on these pathology tasks.

LLaVA-Med [11] struggles with task comprehension. Although LLaVA-Med was included in our initial evaluation due to its medical domain adaptation, its results are omitted from Table 2. Under both zero-shot and one-shot prompting, it consistently failed to perform the classification task effectively, often failing to adhere to the class choices provided, providing blank responses in some cases and for the datasets that it was able to provide relevant output it performed poorly, for instance on Bladder Grade its Cohen’s Kappa score was -0.005, similar trend was followed for other datasets. This suggests its general medical pre-training does not directly equip it for specific cellular/tissue morphology classification via simple prompting and highlights the need for more specialized adaptation or fine-tuning for such tasks.

Performance does not strictly correlate with VLM scale. Interestingly, larger models did not universally outperform smaller ones in our one-shot and zero-shot evaluations. For instance, on the Bladder Grade task, the smaller GPT 4.1 Mini ($\kappa=0.515$) and InternVL3 ($\kappa=0.450$) achieved higher agreement than both the larger GPT 4.1

Model	Bladder Tumor (n=2) (64x64)			Bladder Grade (n=3) (280x280)			Meng [14] <i>et al.</i> (n=3) (128x128)			BCCD [15] (n=4) (320x240)			PanNuke [9] (n=5) (46x46)			Matek [13] <i>et al.</i> (n=10) (250x250)		
	Acc	F1	κ	Acc	F1	κ	Acc	F1	κ	Acc	F1	κ	Acc	F1	κ	Acc	F1	κ
Supervised																		
CNN	0.960	0.960	0.920	0.990	0.990	0.985	0.887	0.886	0.830	0.711	0.710	0.615	0.552	0.518	0.440	0.779	0.734	0.748
Zero Shot																		
GPT 4.1	0.502	0.343	0.005	0.360	0.239	0.040	0.347	0.203	0.020	0.766	0.755	0.688	0.271	0.268	0.089	0.353	0.327	0.280
GPT 4.1 Mini	0.527	0.406	0.055	0.257	0.206	-0.090	0.328	0.328	-0.007	0.646	0.617	0.528	0.203	0.207	0.004	0.234	0.197	0.160
Gemini 2.5 Pro	0.420	0.333	-0.004	0.170	0.167	-0.004	0.088	0.124	-0.004	0.723	0.693	0.635	0.162	0.194	0.066	0.386	0.410	0.331
InternVL3	0.618	0.594	0.235	0.337	0.175	0.005	0.378	0.286	0.068	0.636	0.639	0.515	0.268	0.268	0.085	0.172	0.158	0.095
One Shot																		
GPT 4.1	0.637	0.636	0.275	0.595	0.550	0.393	0.323	0.287	0.004	0.920	0.920	0.893	0.435	0.429	0.294	0.489	0.471	0.422
GPT 4.1 Mini	0.527	0.497	0.055	0.677	0.666	0.515	0.352	0.287	0.028	0.797	0.784	0.730	0.499	0.504	0.374	0.411	0.400	0.332
Gemini 2.5 Pro	0.502	0.499	0.012	0.608	0.590	0.415	0.322	0.270	0.022	0.866	0.863	0.822	0.381	0.362	0.228	0.464	0.470	0.406
InternVL3	0.657	0.656	0.315	0.633	0.637	0.450	0.393	0.384	0.090	0.770	0.763	0.693	0.385	0.381	0.231	0.307	0.332	0.227

Table 2. Performance Comparison of Models Across Datasets and Prompting Regimes (Sorted by Class Count). Best score within each regime (Supervised, Zero Shot, One Shot) is **bolded**. Overall best score is **underlined**.

($\kappa=0.393$) and Gemini 2.5 Pro ($\kappa=0.415$). Similar trends were observed on Bladder Tumor (InternVL3 $\kappa=0.315$ outperformed others) and PanNuke (GPT 4.1 Mini $\kappa=0.374$ was highest). While factors like specific model architectures and pre-training data mixtures play a role, these results suggest that simply scaling model size may not guarantee optimal performance on specialized tasks like histopathology classification, highlighting the potential importance of architectural choices or training data composition even within large foundation models.

VLMs generally achieve better results on datasets with larger image dimensions. Comparing performance across datasets with varying average image sizes (Table 1) reveals a tendency for VLMs to perform better on images with larger pixel dimensions in the one-shot setting. For example, the highest Kappa scores were achieved on BCCD (Avg. 320x240 pixels; best VLM $\kappa=0.893$) and Bladder Grade (Avg. 280x280 pixels; best VLM $\kappa=0.515$). In contrast, performance was generally lower on datasets with smaller average sizes like PanNuke (Avg. 46x46 pixels; best VLM $\kappa=0.374$) and Bladder Tumor (Avg. 64x64 pixels; best VLM $\kappa=0.315$). This aligns with the observation that current general VLM visual encoders might be less adept at capturing the fine-grained details necessary for classification in lower-resolution images compared to tasks involving larger, more distinct objects or scenes.

VLMs show potential, outperforming CNN on a specific task. While the supervised CNN was dominant overall, VLMs demonstrated significant potential on the BCCD dataset. The one-shot GPT 4.1 model achieved the top performance (Acc: 0.920, F1: 0.920, $\kappa=0.893$), surpassing the baseline CNN ($\kappa=0.615$). Several other VLMs also outperformed the CNN on this task in the one-shot setting (e.g., Gemini 2.5 Pro: $\kappa=0.822$). While potentially influenced by the CNN’s small training data size for this specific dataset, this result underscores the potential of VLMs re-

placing CNNs in medical field. It suggests that by leveraging vast prior knowledge, VLMs can achieve high accuracy with minimal examples (one-shot) and also have good performance in zero shot settings, hinting at their promise as potent tools for rapid hypothesis testing or as adaptable ‘digital pathology assistants’ in settings where extensive dataset curation for supervised training is impractical.

4. Conclusion

This study benchmarked the performance of contemporary Vision-Language Models (VLMs), including GPT-4.1, Gemini 2.5 Pro, and InternVL, on diverse histopathology classification tasks using zero-shot and one-shot in-context learning (ICL). Our findings demonstrate that while one-shot prompting significantly enhances VLM performance over zero-shot ($p \approx 1.005 \times 10^{-5}$ based on Kappa scores), indicating the potential of ICL for rapid adaptation, current general-purpose VLMs generally lag behind traditional supervised CNNs trained on these specific tasks. Performance did not strictly correlate with model scale, and VLMs tended to perform better on datasets with larger image dimensions. Notably, VLMs outperformed baseline CNN results on the BCCD datasets highlighting the potential of VLMs in pathological tasks. Overall, this study highlights both the promise of ICL for rapidly applying VLMs to pathology and the current performance gap compared to specialized supervised models. Future work should focus on developing VLMs with enhanced visual understanding tailored to cellular and tissue morphology, potentially through domain-specific pre-training or architectural adaptations, to bridge this gap for reliable diagnostic support.

References

- [1] Jean-Baptiste Alayrac, Jeff Donahue, Pauline Luc, Antoine Miech, Iain Barr, Yana Hasson, Karel Lenc, Arthur

- Mensch, Katie Millican, Malcolm Reynolds, Roman Ring, Eliza Rutherford, Serkan Cabi, Tengda Han, Zhitao Gong, Sina Samangoeei, Marianne Monteiro, Jacob Menick, Sebastian Borgeaud, Andrew Brock, Aida Nematzadeh, Sahand Sharifzadeh, Mikolaj Binkowski, Ricardo Barreira, Oriol Vinyals, Andrew Zisserman, and Karen Simonyan. Flamingo: a visual language model for few-shot learning, 2022. 1
- [2] Peter Bankhead, Maurice B. Loughrey, José A. Fernández, Yvonne Dombrowski, Darragh G. McArt, Philip D. Dunne, Stephen McQuaid, Ronan T. Gray, Liam J. Murray, Helen G. Coleman, Jacqueline A. James, Manuel Salto-Tellez, and Peter W. Hamilton. Qupath: Open source software for digital pathology image analysis. *Scientific Reports*, 7(1), 2017. 2
- [3] Jeffrey L. Bessen, Melissa Alexander, Olivia Foroughi, Roderick Brathwaite, Emre Baser, Liam C. Lee, Omar Perez, and Gary Gustavsen. Perspectives on reducing barriers to the adoption of digital and computational pathology technology by clinical labs. *Diagnostics*, 15(7):794, 2025. 1
- [4] Tom B. Brown, Benjamin Mann, Nick Ryder, Melanie Subbiah, Jared Kaplan, Prafulla Dhariwal, Arvind Neelakantan, Pranav Shyam, Girish Sastry, Amanda Askell, Sandhini Agarwal, Ariel Herbert-Voss, Gretchen Krueger, Tom Henighan, Rewon Child, Aditya Ramesh, Daniel M. Ziegler, Jeffrey Wu, Clemens Winter, Christopher Hesse, Mark Chen, Eric Sigler, Mateusz Litwin, Scott Gray, Benjamin Chess, Jack Clark, Christopher Berner, Sam McCandlish, Alec Radford, Ilya Sutskever, and Dario Amodei. Language models are few-shot learners, 2020. 1
- [5] Zhe Chen, Jiannan Wu, Wenhai Wang, Weijie Su, Guo Chen, Sen Xing, Muyan Zhong, Qinglong Zhang, Xizhou Zhu, Lewei Lu, et al. Internvl: Scaling up vision foundation models and aligning for generic visual-linguistic tasks. In *Proceedings of the IEEE/CVF Conference on Computer Vision and Pattern Recognition*, pages 24185–24198, 2024. 1, 3
- [6] Google DeepMind. Gemini: A family of highly capable multimodal models. <https://arxiv.org/abs/2312.11805>, 2023. 1, 3
- [7] Haodong Duan, Junming Yang, Yuxuan Qiao, Xinyu Fang, Lin Chen, Yuan Liu, Xiaoyi Dong, Yuhang Zang, Pan Zhang, Jiaqi Wang, et al. Vlmevalkit: An open-source toolkit for evaluating large multi-modality models. In *Proceedings of the 32nd ACM International Conference on Multimedia*, pages 11198–11201, 2024. 3
- [8] Dyke Ferber, Georg Wölflein, Isabella C. Wiest, Marta Ligeró, Srividhya Sainath, Narmin Ghaffari Laleh, Omar S. M. El Nahhas, Gustav Müller-Franzes, Dirk Jäger, Daniel Truhn, and Jakob Nikolas Kather. In-context learning enables multimodal large language models to classify cancer pathology images. *Nature Communications*, 15(1), 2024. 1
- [9] Jevgenij Gamper, Navid Alemi Koohbanani, Ksenija Benes, Ali Khuram, and Nasir Rajpoot. Pannuke: an open pan-cancer histology dataset for nuclei instance segmentation and classification. In *European Congress on Digital Pathology*, pages 11–19. Springer, 2019. 2, 4
- [10] Grégoire Gessain and Magali Lacroix-Triki. Computational pathology for breast cancer: Where do we stand for prognostic applications? *The Breast*, 81:104464, 2025. 1
- [11] Chunyuan Li, Cliff Wong, Sheng Zhang, Naoto Usuyama, Haotian Liu, Jianwei Yang, Tristan Naumann, Hoifung Poon, and Jianfeng Gao. Llava-med: Training a large language-and-vision assistant for biomedicine in one day. *arXiv preprint arXiv:2306.00890*, 2023. 2, 3
- [12] Anant Madabhushi and George Lee. Image analysis and machine learning in digital pathology: Challenges and opportunities. *Medical Image Analysis*, 33:170–175, 2016. 1
- [13] Christian Matek, Susanne Krappe, Christian Münzenmayer, Torsten Haferlach, and Carsten Marr. An expert-annotated dataset of bone marrow cytology in hematologic malignancies. <https://doi.org/10.7937/TCIA.AXH3-T579>, 2021. The Cancer Imaging Archive. 2, 4
- [14] Nan Meng, Edmund Lam, Kevin Kin Man Tsia, and Hayden Kwok-Hay So. Human somatic label-free bright-field cell images, 2018. 2, 4
- [15] Paul Timothy Mooney. Blood cell images. <https://www.kaggle.com/datasets/paultimothymooney/blood-cells>, 2018. Accessed: 2025-04-27. 2, 4
- [16] Sandra Morales, Kjersti Engan, and Valery Naranjo. Artificial intelligence in computational pathology – challenges and future directions. *Digital Signal Processing*, 119:103196, 2021. 1
- [17] Harsha Nori, Yin Tat Lee, Sheng Zhang, Dean Carignan, Richard Edgar, Nicolo Fusi, Nicholas King, Jonathan Larson, Yuanzhi Li, Weishung Liu, Renqian Luo, Scott Mayer McKinney, Robert Osazuwa Ness, Hoifung Poon, Tao Qin, Naoto Usuyama, Chris White, and Eric Horvitz. Can generalist foundation models outcompete special-purpose tuning? case study in medicine, 2023. 1
- [18] OpenAI. Gpt-4 technical report. <https://doi.org/10.48550/arXiv.2303.08774>, 2023. 1, 3
- [19] Keiron O’Shea and Ryan Nash. An introduction to convolutional neural networks, 2015. 2
- [20] Joon Sung Park, Joseph C. O’Brien, Carrie J. Cai, Meredith Ringel Morris, Percy Liang, and Michael S. Bernstein. Generative agents: Interactive simulacra of human behavior, 2023. 2
- [21] Alec Radford, Jong Wook Kim, Christopher Hallacy, Aditya Ramesh, Gabriel Goh, Sandhini Agarwal, Girish Sastry, Amanda Askell, Pamela Mishkin, Jack Clark, Gretchen Krueger, and Ilya Sutskever. Learning transferable visual models from natural language supervision. In *Proceedings of the 38th International Conference on Machine Learning (ICML)*, pages 8748–8763. PMLR, 2021. 1
- [22] Muhammad Shaban, Ruqayya Awan, Muhammad Moazam Fraz, Ayesha Azam, David Snead, and Nasir M. Rajpoot. Context-aware convolutional neural network for grading of colorectal cancer histology images, 2019. 1